3D modeling of buried valley geology using airborne electromagnetic data

Vincenzo Sapia[1], Greg A. Oldenborger[2], Flemming Jørgensen[3], André J.-M. Pugin[2], Marco Marchetti[1], and Andrea Viezzoli[4]

Abstract

Buried valleys are important hydrogeologic features of glaciated terrains. They often contain valuable groundwater resources; however, they can remain undetected by borehole-based hydrogeologic mapping or prospecting campaigns. Airborne electromagnetic (AEM) surveys provide high-density information that can allow detailed features of buried valleys to be efficiently mapped over large geographic areas. Using AEM data for the Spiritwood Valley Aquifer system in Manitoba, Canada, we developed a 3D electric property model and a geologic model of the buried valley network. The 3D models were derived from voxel-based segmentation of electric resistivity obtained via spatially constrained inversion of two separate helicopter time-domain electromagnetic data sets (AeroTEM and versatile time-domain electromagnetic [VTEM]) collected over the survey area. Because the electric resistivity do not provide unequivocal information on subsurface lithology, we have used a cognitive procedure to interpret the electric property models of the aquifer complex, while simultaneously incorporating supporting information for the assignment of lithology in the 3D geologic model. For the Spiritwood model, supporting information included seismic reflection data and borehole records. These data constrained valley geometry and provided lithologic benchmarks at specific borehole sites and along seismic transects. The large-scale AeroTEM survey provided the basis for modeling the regional extent and connectivity of the Spiritwood Valley Aquifer system, whereas the local-scale VTEM survey provided higher near-surface resolution and insight into a detailed shallow architecture of individual buried valleys and their fill.

Introduction

The importance of buried valleys as groundwater resources is well known to geologists, hydrogeologists, and geophysicists studying glaciated terrain (e.g., Cummings et al., 2012). As groundwater demand increases, several countries around the world are promoting hydrogeologic studies to adequately map buried valley aquifers (Kluiving et al., 2003; Sheets and Bossenbroek, 2005; Gunnik et al., 2012; Jørgensen et al., 2013; Pugin et al., 2014). Lithological information on buried valleys is usually derived from water well records or other drilled borehole records (e.g., Jørgensen et al., 2003). A more thorough understanding of buried valley occurrence, depth, architecture, and fill sequence can be obtained by integrating geophysical data, such as time-domain electromagnetics (TEM), ground-based (Auken et al., 2003; Danielsen et al., 2003; Jørgensen et al., 2003, 2005) and airborne (Auken et al., 2008; Oldenborger et al., 2013). Many authors have also demonstrated the use of seismic methods as an effective tool for buried valley mapping in conjunction with TEM data (Gabriel et al., 2003; Jørgensen et al., 2003; Høyer et al., 2011; Oldenborger et al., 2013; Pugin et al., 2014).

Buried valleys often result in a complex aquifer architecture with numerous cross-cutting features occurring over several generations (Jørgensen and Sandersen, 2006). As such, high data density and accurate 3D data representation are crucial for their complete understanding. Many geologic models are based on water well data exclusively (Venteris, 2007), or on a combination of borehole data and geologic and/or seismic cross sections (Kaufmann et al., 2008; Scharling et al., 2009; Royse, 2010; Raiber et al., 2012). However, borehole and ground-based geophysical data sources are often too sparse for continuous 3D representation of complex geology at regional scales (Jørgensen et al., 2009; Sapia et al., 2014b). Water well records are widespread and readily available; however, in addition to being similarly

[1]Istituto Nazionale di Geofisica e Vulcanologia, Rome, Italy. E-mail: vincenzo.sapia@ingv.it; marco.marchetti@ingv.it.
[2]Geological Survey of Canada, Natural Resources Canada, Ottawa, Ontario, Canada. E-mail: greg.oldenborger@nrcan-rncan.gc.ca; andre.pugin@nrcan-rncan.gc.ca.
[3]Geological Survey of Denmark and Greenland, Højbjerg, Denmark. E-mail: flj@geus.dk.
[4]Aarhus Geophysics Aps, Aarhus, Denmark. E-mail: andrea.viezzoli@aarhusgeo.com.

Manuscript received by the Editor 27 May 2015; revised manuscript received 23 July 2015; published online 23 September 2015. This paper appears in *Interpretation*, Vol. 3, No. 4 (November 2015); p. SAC9–SAC22, 14 FIGS.
http://dx.doi.org/10.1190/INT-2015-0083.1.

sparse, they may also be of low or unknown quality (Jørgensen et al., 2009; Oldenborger et al., 2014; Logan et al., 2015). In contrast, airborne electromagnetic (AEM) surveys provide high data density quickly and economically over large geographic areas. In particular, helicopter time-domain electromagnetic (HTEM) systems benefit from small footprints and near surface data (Paine and Minty, 2005; Allard, 2007; Thomson et al., 2007; Fountain et al., 2008; Sattel, 2009; Schamper et al., 2014). However, unlike the mineral exploration environment with large contrasts in electric resistivity between ore zones and host rock, the resistivity contrast between aquitard and aquiclude is relatively small, thus complicating the ability to accurately discriminate groundwater resources. Resistivity mapping in a groundwater application, requires careful attention to data processing, calibration, and inversion (Foged et al., 2013; Viezzoli et al., 2013; Podgorsky et al., 2013; Sapia et al., 2014a)

AEM data or inversion results can be used in the construction of conceptual or process models (e.g., Pugin et al., 2014), but they do not necessarily yield a conclusive or unique lithological or geologic model. Nevertheless, the unparalleled spatial density of AEM data can be invaluable in 3D model building (Berg et al., 2011; Høyer et al., 2015; Jørgensen et al., 2015). The implementation of AEM-based geologic modeling in recent literature varies from semiautomated or geostatistical approaches (Gunnink et al., 2009, 2012; Marker et al., 2014) to knowledge-driven or cognitive approaches (Jørgensen et al., 2010, 2013). Automated or geostatistical approaches are limited by the nonunique relationship between resistivity and lithology. Often, the highest degree of segmentation that can be achieved is of overburden/bedrock (Oldenborger et al., 2014) or aquifer/aquitard (Christiansen et al., 2014). Conversely, the cognitive approach uses expert knowledge and allows for the simultaneous consideration of complex aspects regarding the physical properties of the subsurface and the limitations of the applied methods. The resulting models can be unlimited in detail and can incorporate existing geologic information of all forms. The drawback is that cognitive models are labor intensive and may be difficult to reproduce.

We demonstrate the utility and flexibility of 3D AEM-based cognitive geologic modeling for the Spiritwood Valley Aquifer system in Manitoba, Canada, using two HTEM data sets: a regional AeroTEM III data set (Oldenborger et al., 2013) and a localized versatile time-domain electromagnetic (VTEM) data set (Legault et al., 2012). The AeroTEM and VTEM data sets are processed and inverted to obtain resistivity models of the subsurface. With the resistivity models, we use 3D voxel-based segmentation to construct an electric property model of the buried valley network. During the voxel-based modeling, seismic data and borehole logs are used to aid interpretation of buried valley geometry and to guide a user-driven cognitive interpretation of lithology.

Key features of the regional geologic model include the bedrock topography (considered as the primary aquiclude at depth), the distribution of glacial till that forms a near-surface aquitard, the distribution and connectivity of high-porosity materials with aquifer potential, and the occurrence of potential recharge pathways. Given the localized nature of the VTEM data, they are used only to interpret additional details of resistivity structure in the shallow subsurface of the aquifer system.

Study area

The Spiritwood study area in southern Manitoba is part of a buried valley aquifer system that extends from Manitoba, across North Dakota and into South Dakota within a regional till plain (Winter et al., 1984). Stratigraphy in the region is variable, but includes multiple till units, and intertill sands and gravels over shale bedrock (Randich and Kuzniar, 1984). Data in Manitoba include water well records and some geotechnical boreholes (Wiecek, 2009; Crow et al., 2012) and geophysical surveys including two separate HTEM surveys (Legault et al., 2012; Oldenborger et al., 2013).

Geologic setting

Buried valleys are common features in glacial terrain of the Canadian Prairies. Numerous valleys were cut into Cretaceous and Tertiary bedrock units prior to continental glaciations, mainly where the underlying bedrock consists of easily eroded sedimentary rock, such as shale (Betcher et al., 2005). Alluvial deposits are generally thought to have been transported from the Rocky Mountains to the west and rest on the underlying bedrock in parts of many of these valleys. Considerable modification occurred to many of the older valleys and their fill during the Pleistocene; new valleys were formed by meltwater erosion during glacial retreats and several generations of till were deposited (Shaver and Pusc, 1992). By the end of the Pleistocene, many of the valleys had been partially or completely filled with glacial sediments.

Cummings et al. (2012) present a conceptual geologic model for Prairie buried valley incision, addressing Rocky Mountain clast provenance as one of the main criteria used to interpret subaerial preglacial origin of buried valleys, although this is complicated by tectonic uplift and subsequent erosion. Buried valleys that contain Precambrian Shield clasts along their bases and stratigraphically overlie till, are commonly inferred to have been incised by proglacial meltwater streams (Kehew et al., 1986). Buried valleys within till and bedrock that exhibit upslope trends, undulating profiles and abrupt terminations may be interpreted as tunnel valleys (Pugin et al., 2014). The term tunnel valley refers to valleys formed by subglacial meltwater erosion driven by hydrostatic pressure gradients (Jørgensen and Sandersen, 2006).

Helicopter time-domain electromagnetic surveys

The Spiritwood HTEM surveys are an AeroTEM survey (Aeroquest, Ltd.) and a VTEM survey (Geotech, Ltd.). The AeroTEM survey consists of 3000-line km of HTEM

data acquired over several flights. Flight lines were spaced at 400 m and oriented southwest–northeast to cover an area of approximately 1062 km^2 (Figure 1). The data were collected using 17 variable width off-time gates from 70 μs to 3 ms. The VTEM flight lines were strategically located to coincide with existing seismic reflection profiles (Figure 1). The VTEM data consist of 44 time gates from 20 μs to 9 ms after turn-off. AeroTEM and VTEM data were inverted using a spatially constrained, smoothed least-squares inversion, in which the system's specifications are modeled (Viezzoli et al., 2008). The result of the inversion is a set of 1D models with 29 logarithmically spaced layers of electric resistivity spaced at approximately 30 m along each flight line (Sapia et al., 2014a, 2014b). Due to removal of noisy data, larger spacing between 1D models can occur. The data were also inverted using a four-layer blocky parameterization with lateral and vertical constraints on the model resistivity and layer thickness. Resistivity maps at different elevations are shown in Figure 2 that clearly show the existence of moderately resistive, regional-scale features elongated in the northwest–southeast direction interpreted as the Spiritwood buried valley, which has been attributed to preglacial fluvial erosion (Cummings et al., 2012). The Spiritwood valley is set in a conductive background interpreted to be the Cretaceous shale bedrock (Randich and Kuzniar, 1984; Betcher et al., 2005). Two narrow resistive features within the Spiritwood valley (Figure 2c) are interpreted to be incised valleys of proglacial origin (Pugin et al., 2014). In addition to the two distinct incised valleys, a complex network of resistive valley-like features is observed inside and outside the Spiritwood valley interpreted as subglacial tunnel valleys (Pugin et al., 2014). The network of cross-cutting buried valleys at different elevations with different widths and depths reveals a complex glacial setting.

A cross section of the AeroTEM and VTEM resistivity models along the southern seismic profile (S1, Figure 1) is shown in Figure 3 along with supporting seismic information. The two models reveal different pictures of the subsurface due to the differences in resolution and timing between the two data sets (Sapia et al., 2014a). Estimated errors on seismic depth to bedrock resolution are approximately 10% due to variations in velocity and picking accuracy (Oldenborger et al., 2013). Although the AeroTEM model provides us with regional-scale information, its relatively late early-time gates result in limited near-surface information. The AeroTEM model lacks a surficial resistor, whereas the VTEM model exhibits the sequence of resistor-conductor-resistor-bedrock ob-

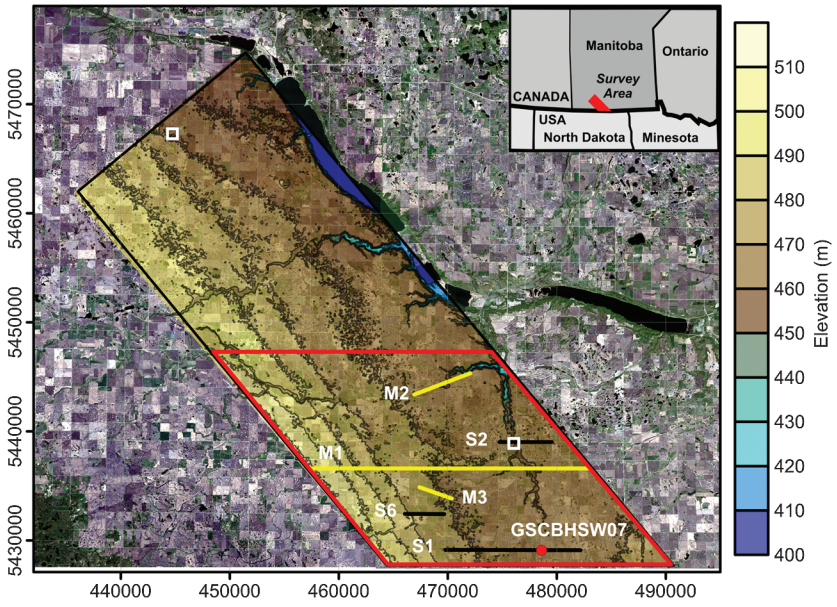

Figure 1. Location and digital elevation model of the Spiritwood AeroTEM survey area in southern Manitoba, Canada. Black lines indicate locations of seismic reflection profiles. The VTEM survey consists of three parallel lines along seismic profile S1. The red dot indicates location of a cored borehole. White squares indicate locations of ground TEM soundings. Yellow lines indicate locations of model cross sections to be discussed. The red box indicates the boundary of the 3D model.

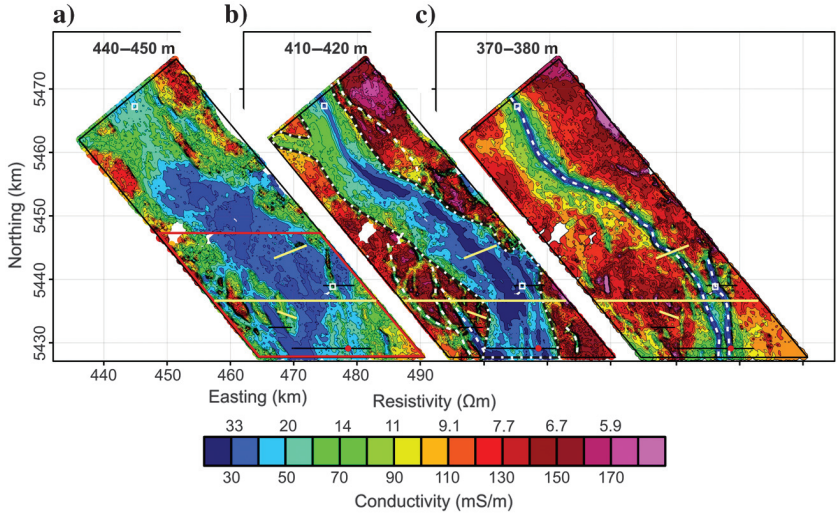

Figure 2. Inversion results for the AeroTEM survey. The recovered 1D resistivity models are interpolated as resistivity maps at different elevation intervals: (a) 440–450 m, (b) 410–420 m, and (c) 370–380 m. Dashed black lines depict the interpreted extent of the broad Spiritwood valley; dashed white lines depict the interpreted axes of several narrower valleys. The red box indicates the boundary of the 3D model.

served in the borehole geophysical log along S1. The VTEM model exhibits more detailed delineation of the very near surface, including good agreement with a shallow intertill transition identified in the seismic data. Both models exhibit a clear decrease in resistivity at the shale surface as interpreted from the seismic data. However, the AeroTEM data lack the power or signal-to-noise ratio level required to recover the bottom of the incised valleys and the VTEM data result in overestimation of the depth of the incised valleys, possibly due to 3D effects on the 1D forward model in the inversion (Goldman et al., 1994).

Methods

3D modeling procedure

The first step in our modeling procedure involves 3D visualization of the AEM inversion results. We follow the procedure described by Jørgensen et al. (2013). The collection of 1D models are first interpolated to regular depth and elevation intervals (5 m), and then interpolated in 2D via Kriging on a regular grid (100-m spacing) to yield resistivity maps at common depths and elevations. These maps are then stacked to generate a pseudo-3D resistivity model that can be interrogated at any point (the model exists in 3D, but was built using 1D physics with 3D constraints and 2D interpolation). Alternative gridding procedures are possible (Pryet et al., 2011), but we find that our method provides the most accurate representation of the original 1D models. Interpolation acts to fill any gaps caused by removal of noisy soundings based on the adopted search radius, but the weakness caused by the lack of data in these areas must be taken into account during modeling.

The second step in our modeling procedure involves assignment of an electric property model. The cognitive modeling approach and the concept of 3D voxel modeling are discussed in detail by Jørgensen et al. (2013). The modeling is performed by selection of voxel groups, which define a volumetric shape in the output 3D model. Voxel modeling is particularly applicable to the complex geology found in glaciated environments, which is rarely organized in well-defined horizontal layers and which often includes multiple cross-cutting buried valleys of different generations. The initial assignment of electric properties is accomplished primarily through the use of region-growing techniques (Jørgensen et al., 2013). The selected volume of voxels is then attributed with a common property according to the geophysicists or geologist's interpretation. Simultaneous with region growing, upper and lower boundaries of the volume are constrained by surfaces that represent geologic contacts or unconformities. These surfaces are built from handmade control points produced from cognitive interpretation of the resistivity model and seismic data. A large number of the interpreted buried valleys occur as elongated features with significant resistivity contrast in comparison with the conductive shale bedrock (such as the two incised valleys in Figure 2c). Despite substantial variability along the axes of these valleys, they are easily recognizable in the re-

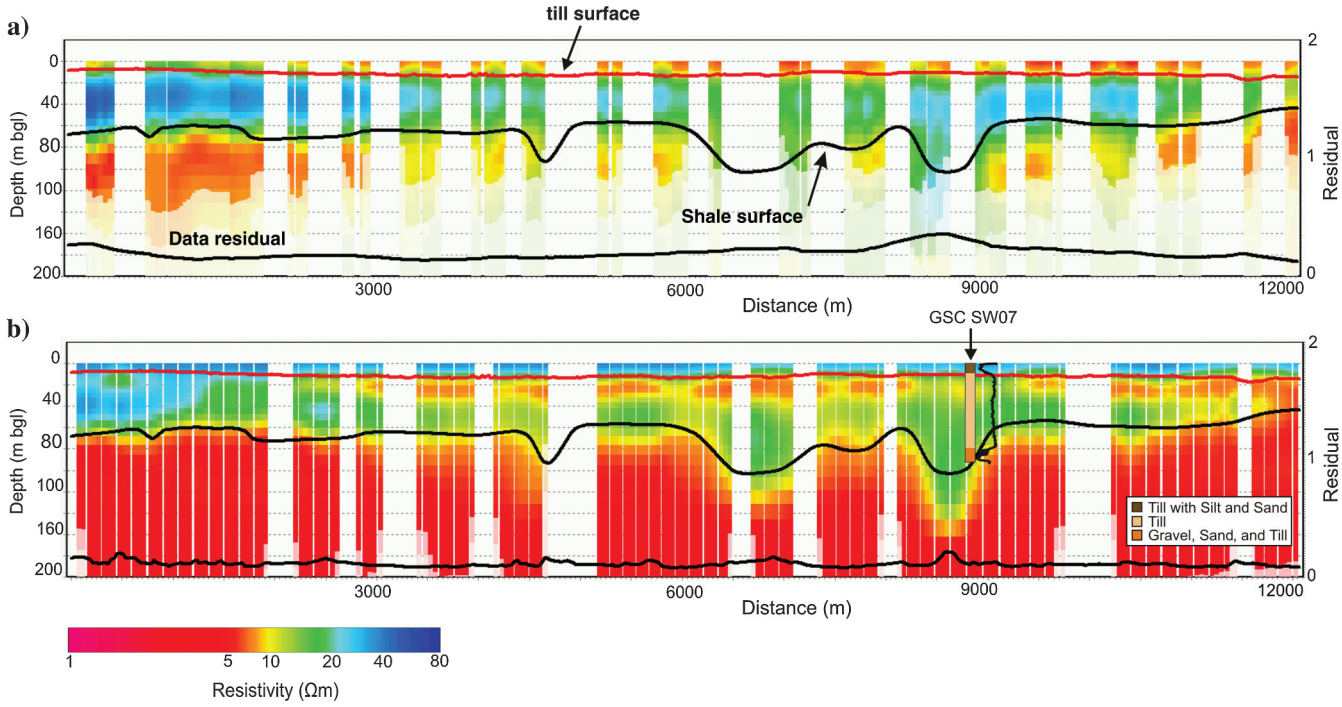

Figure 3. (a) AeroTEM and (b) VTEM resistivity models along seismic line S1. The red line is an interpreted intertill reflection surface. The upper black line marks a seismic reflection facies change interpreted as the bedrock surface (Pugin et al., 2011). The lower black line is the data misfit. A simplified stratigraphic description and the electromagnetic conductivity log are shown for borehole GSC-BH-SW07 (Crow et al., 2012).

sistivity model and control points are manually selected to define the erosional surface of these valleys. However, many of the interpreted tunnel valleys exhibit minimal resistivity contrast and require careful attention. Numerous profiles of the smooth and blocky 3D resistivity models are examined along different orientations in conjunction with seismic data, other ground geophysical data, and the conceptual knowledge of valley shapes. The smooth inversion better defines spatial variations and provides a more realistic image of the complex morphologies. However, the blocky inversion helps to locate distinct layer boundaries, which are crucial for defining bounding surfaces. Joint interpretation of all available data is time consuming, but it allows for additional details not available from the AEM results alone and ensures a consistent model.

Interpretation of lithology

The final step in the modeling procedure is to assign lithology to the specific regions of the electric property model. Direct classification or learning-based methods might be appropriate given a large amount of quality training data (Gunnink and Bernhard, 2015). However, the water well records available for the Spiritwood are limited in quality and spatial accuracy (Sapia et al., 2014b). Alternatively, water well data are used indirectly along with all other sources of information to assign lithology.

In general, our modeling effort is guided by the observed relative classification of conductive shale bedrock (5–15 Ωm), moderately conductive till packages (15–30 Ωm), and resistive sand and gravel (>30 Ωm) derived from water well and borehole information, as well as ground-based electric and electromagnetic surveys (Crow et al., 2012; Oldenborger et al., 2013, 2014; Oldenborger and Brewer, 2014). The resistivity ranges for Spiritwood tills, and for the sand and gravel, are somewhat lower than expected for typical glacial sediments (e.g., Palacky, 1988), and we attribute this to a dominantly shale provenance as opposed to a granitic Canadian Shield provenance (e.g., Cummings et al., 2012). Variations in resistivity can also result from variable pore water conductivity, but for this work, we make the assumption that pore water conductivity is essentially constant within each lithological unit.

Results

The resistivity model derived from AeroTEM survey inversion exhibits a bimodal distribution (Figure 4). Peak resistivities are approximately 8 and 20 Ωm, which we attribute to the shale bedrock and the regional heterogeneous diamicton valley fill, respectively. We consider the observed high resistivities (>35 Ωm) to be representative of sand and gravel. The nonunique relationship between lithology and resistivity and the smooth inversion model make direct model segmentation difficult. This fact is illustrated in Figure 5 by the result of a simple automatic segmentation into a model consisting of bedrock aquiclude, till aquitard, and sand/gravel aquifer using the nonoverlapping classes of <15, 15–30 , and >30 Ωm. The relatively high threshold for bedrock resistivity is required to match water well and seismic observations (Figure 3). This is the first weakness of automatic segmentation that reflects the fact that, for a smooth model, the bedrock surface may not be represented by the true bedrock resistivity, but rather, a transitional value. This necessarily elevated bedrock resistivity in turn results in indiscriminate grouping of bedrock and surficial sediments (Figure 5a). This can be remedied by an upward-looking classification algorithm (e.g., Oldenborger et al., 2014), but the problem with nonunique resistivity classification is evident. Finally, automatic segmentation results in buried valley aquifers that are overlain and underlain by till aquiclude. This may be a reality, but based on the resulting valley morphologies (Figure 5c) and other data, we reject this result of automatic segmentation.

AeroTEM modeling

As opposed to direct segmentation based solely on resistivity, cognitive voxel-based modeling provides a method for segmenting the electric resistivity model with subtle, nonunique and spatially dependent, or sequence-dependent relationships between electric properties and lithology. In addition, we incorporate bounding constraint surfaces that add a process-based element of erosional unconformities to the model. To segment the Quaternary sequence, the buried valleys and the bedrock, we investigate the whole resistivity model by examining several profiles at different orientations that cross different valley features (Figures 1 and 2). Several examples follow.

To interpret the incised valleys, we used control points to define the erosional surface of the resistive valley feature within the conductive bedrock as shown in Figure 6 for model cross section M2 along the western incised valley. In this case, we observe resistivity values greater than 30 Ωm, which we attribute to sand and gravel valley fill. In contrast, while still readily apparent

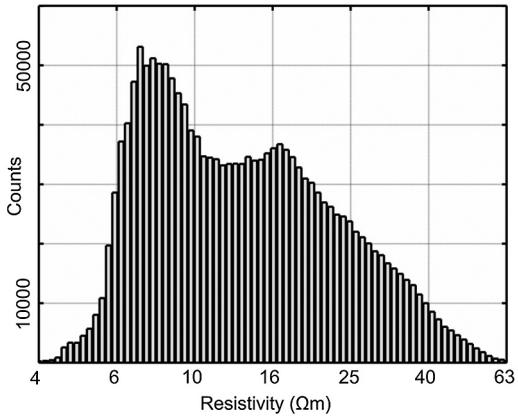

Figure 4. Histogram of layer resistivities for all 1D 29-layer smooth inverse models of the AeroTEM survey (no correction for variable layer thickness).

as a resistive feature in the landscape, the eastern incised valley is less resistive. The differences between the western and eastern incised valleys are corroborated by ground-based TEM surveys, which suggest a more conductive eastern valley fill (Figure 7). This variability may result from a change in pore water chemistry (which we have assumed constant) or from a change in valley fill. We interpret the difference in resistivity to be due to a transition in valley fill from sand and gravel to sandy/silty till or till with smaller amounts of sand and gravel as indicated by cored borehole results along seismic line S1 (Crow et al., 2012).

We interpret the tunnel valleys in a similar fashion to the incised valleys, although the valleys are smaller and the resistivity contrasts are weaker and more variable. Some of the tunnel valleys appear as clear resistive features (>40 Ωm), which we classify as having sand and gravel fill. Conversely, some of these valleys exhibit a resistivity structure as shown in Figure 8. In this case, the contrast is reduced, but the valley is still clearly evident with the resistivity of the fill material ranging from approximately 12–25 Ωm. Valleys that appear to have resistivity on the low end of this range are interpreted as mud-rich till. Valleys that are observed to have resistivity on the high end of this range are interpreted to be filled with sandy\silty till materials.

The final step of the model construction is a definition of the bedrock surface that defines the regional aquiclude. Due to the erosional nature of the environment, we must pay careful attention that the bedrock surface and the subbedrock erosional surfaces identified previously are consistent. To this end, the bedrock surface is first defined using bottom-up region grow

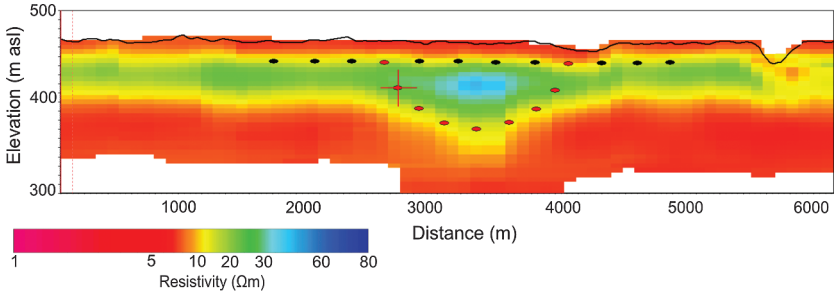

Figure 6. AeroTEM resistivity along model cross section M2. Solid black line is the surface topography. Red dots mark the control points interpreted from the resistivity model to define the bottom erosional surface of the western inset valley. Black dots mark the control points interpreted to define the erosional surface that forms the upper limit of the buried valley.

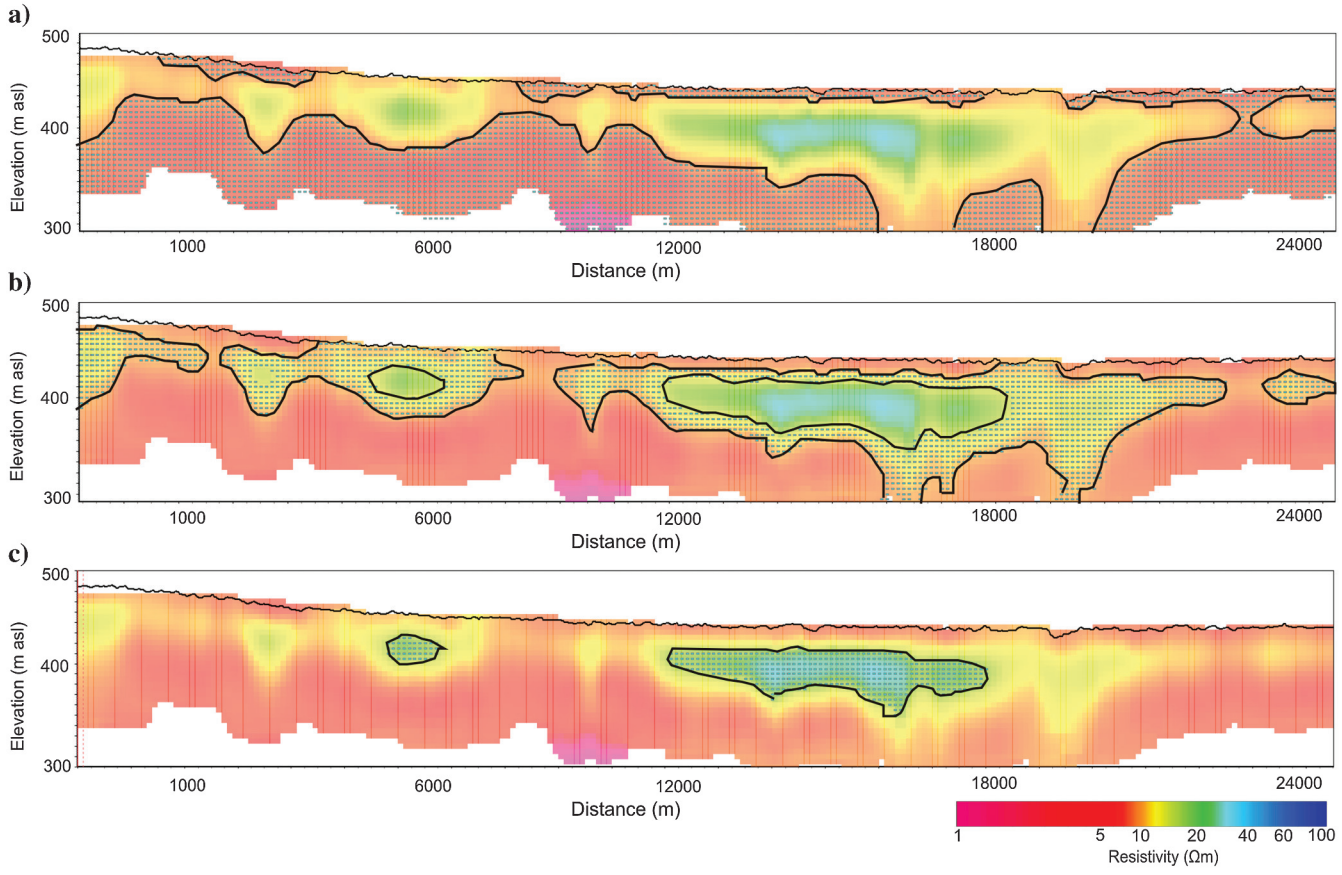

Figure 5. Automatic segmentation of lithology for model cross section M1 based on resistivity thresholds. (a) Bedrock: $5 < \rho < 15$ Ωm, (b) aquitard: $15 < \rho < 30$ Ωm, and (c) aquifer: $\rho < 30$ Ωm.

with a resistivity limit of 15 Ωm. The control points defining the bottom erosional surfaces of all valley features are then interpolated across the model region (Figure 9). Any observation of an interpreted erosional surface below the preliminary bedrock surface becomes the new bedrock surface. However, any interpreted erosional surface above the preliminary bedrock surface is regarded as eroding into unlithified sedimentary material. The resulting bedrock topography is illustrated in Figure 10.

Classification

Having constructed the geometry of the valley structures and the bedrock topography, the valley fill and surrounding material must then be classified. We observe that the main Spiritwood Valley is characterized by highly variable resistivity values that we interpret to represent different types and generations of glacial sediments, mainly till with intertill sands. The dominant resistivity outside the interpreted buried valleys is approximately 14–23 Ωm, which we consider to be representative of the regional till package that extends to approximately 70 m thick. For modeling purposes, we assign the entire sedimentary sequence above bedrock and outside of the interpreted valleys as a general "till." We recognize that this model unit is actually comprised of multiple glacial deposits, but we lack the resolution in our data to discriminate this unit to any degree.

Examples of the results for our 3D modeling approach are shown for the eastern incised valley and a prominent tunnel valley in Figure 11. The buried valleys are observed in the seismic data as a low- to high-amplitude discontinuous reflection facies, and the interpreted bedrock surface is derived from the transition to low-amplitude reflections with limited penetration (Pugin et al., 2014). A gravel surface is interpreted in the seismic data from multiple high-amplitude reflections, whereas the overlying till package manifests as high-amplitude, continuous reflections (Pugin et al., 2011). The bedrock is readily apparent in the AEM resistivity model as a conductive basement overlain by more resistive materials. In general, the AEM result shows good agreement with the seismic information in terms of depth to bedrock, although, due to the smoothing constraints of the spatially constrained inversion, the AeroTEM resistivity model lacks a 500 m wide buried valley as depicted in the seismic 2D profile (Figure 11a, left). In some cases, there is no indication of a valley bottom in the resistivity model despite a corresponding strong change in reflection facies (Figure 11a, left compared with 11b left). For the buried valleys infill materials, the lower resistive response was assigned to a sandy\silty till infill, whereas the higher resistivity values were assigned to gravel and sand sediments (Figure 11c).

Figure 12 shows the final result of the modeling procedure, where the different type of valleys, the bedrock and the general till package are illustrated. The valleys

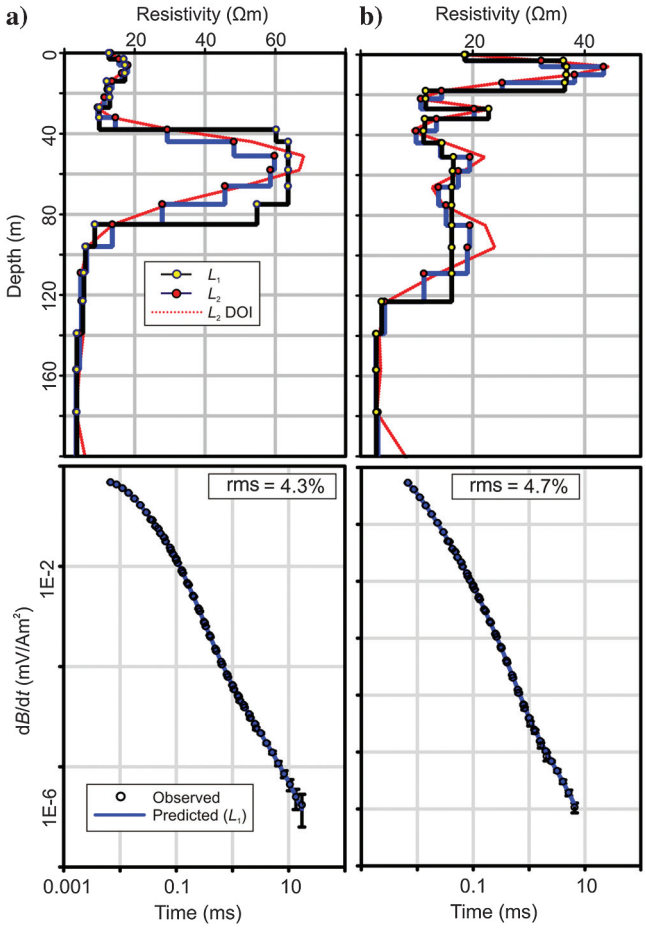

Figure 7. Ground-based TEM data and inversion results for 80 × 80 m central loop soundings (Oldenborger and Brewer, 2014). Data have been inverted using EM1DTM (Farquharson et al., 1993). (a) Western incised valley at the north end of the survey area. (b) Eastern incised valley along S2. The red line indicates model uncertainty as per the depth of investigation index (departure of the red line from the models indicates higher uncertainty).

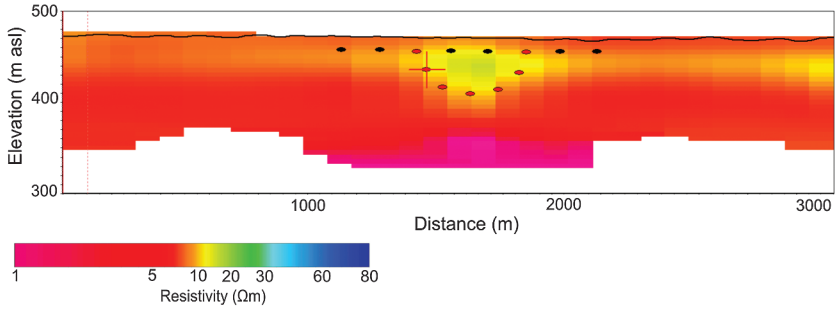

Figure 8. AeroTEM resistivity along model cross section M3. The solid black line is the surface topography. Red dots mark the control points interpreted from the resistivity model to define the bottom erosional surface of this tunnel valley, and black dots mark the control points interpreted to define the erosional surface that forms the upper limit of the valley.

are generally between 30 and 60 m deep and most reach the bedrock in their deeper part. They appear to be U-shaped, and they are 1–2 km wide. All of the valleys are covered by the general till, thus they do not reach the surface. From Figure 10, it is clear that they, like tunnel valleys in general, undulate along their thalwegs. They also show abrupt terminations. The infill sediments vary from gravel and sand, mud-rich till, to sandy/silty till. Sometimes it was possible to resolve more than just one sediment type in the individual valleys (Figure 12).

VTEM modeling

We approach the VTEM resistivity model using the same procedure presented for the AeroTEM survey. To obtain a better match near the surface with available ancillary information available (i.e., electrical resistivity

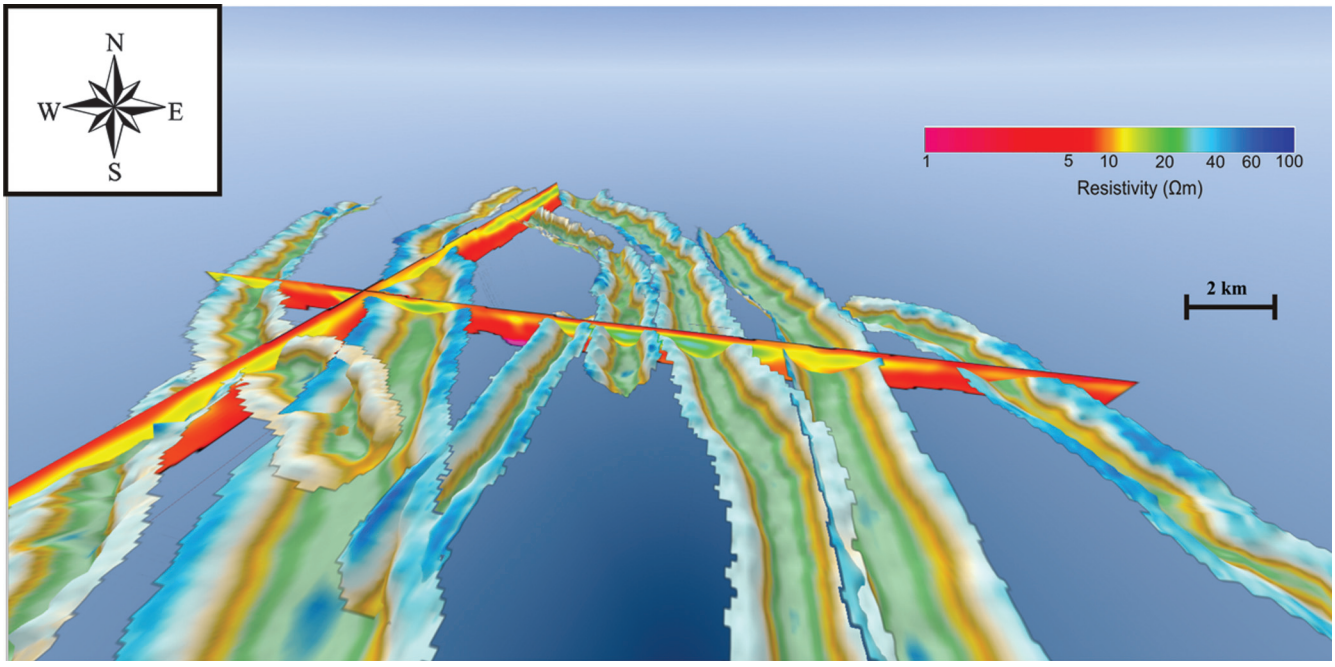

Figure 9. A 3D depiction of the bottom erosional surfaces of all buried valleys interpreted over the entire model volume from the AeroTEM resistivity model (red box in Figures 1 and 2). The surfaces are interpolated from control points using kriging with a search radius of 100 m.

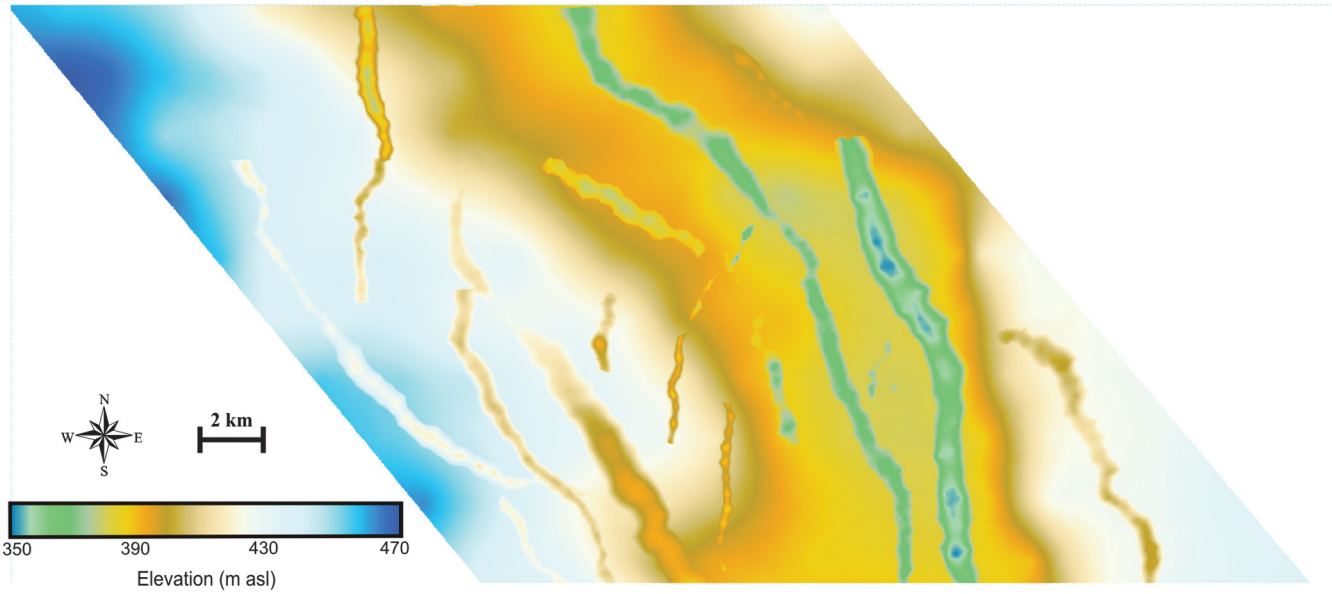

Figure 10. Bedrock topography of the 3D geologic model obtained via interpretation of the AeroTEM resistivity model.

tomography), the VTEM data went through a calibration procedure (Sapia et al., 2014a). First, dominant resistivity contrasts are used to interpret valley surfaces that are interpolated across the model domain. Second, those surfaces are used to constrain voxel-based segmentation in conjunction with definition of the bedrock topography. The resulting voxel-based lithological property model is shown in Figure 13, where the lithology is interpreted based on observed-resistivity values.

Although limited in lateral extent, the VTEM resistivity model provides additional model detail, particularly for the very near surface and the till package. The VTEM data reveal a conductive layer (10 Ωm) at approximately 10 m depth within the till package (Figure 13a). Two surfaces are constructed to constrain the top and the bottom of this interpreted mud-rich intertill unit (Figure 13b). This unit is situated stratigraphically on top of the two incised valleys (Figure 13c). Although the VTEM model provides us with better near surface resolution, it is interesting to note that the VTEM model does not clearly resolve the small tunnel valley that occupies the eastern incised valley as recovered from the AeroTEM model (Figure 12b). In addition, for the VTEM resistivity model, it is not apparent that the same resistivity variability exists between the eastern and the western incised valleys as it does in the AeroTEM model. The two main incised valleys appear to have nearly the same resistivity values. We suspect this may be due to the 2D nature of the VTEM survey data and the resulting inability to represent the regional geologic signature. We observe that the eastern incised valley exhibits moderate resistivity. Guided by our previous AeroTEM modeling and the borehole record, we attribute this to be the response of silty till valley fill. Conversely, the western buried valley is characterized by a slightly higher resistivity, which we attribute to gravel and sand.

Discussion

A 3D representation of the complete geologic model is shown in Figure 14 with the till package stripped away to reveal the interpreted buried valley network. The geologic modeling procedure presented here is generally predicated on the assumption that changes in electric resistivity represent changes in lithology. We use a cognitive voxel-based approach as a means of addressing uncertainty associated with the direct classification of the resistivity model (i.e., nonunique electric properties and model smoothness). With this approach, we are able to distinguish features with minimal contrasts in electric properties or contrasts that are variable geospatially, and are thus only well-defined in a local context. Nevertheless, our approach remains unable to capture all of the variability of the system at scales below our resolving capability, or for features

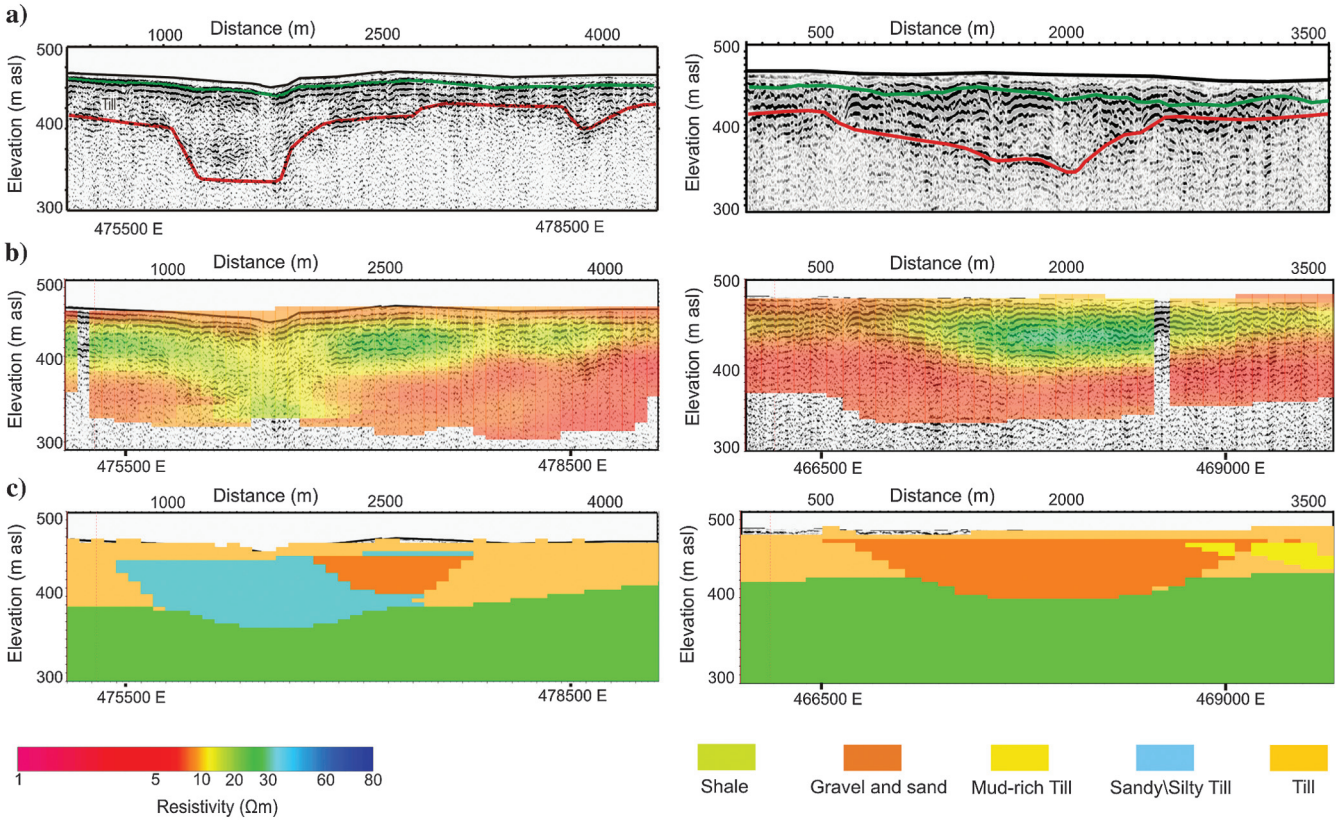

Figure 11. (a) Seismic reflection profiles S2 (left) and S6 (right). Red lines indicate the interpreted bedrock surface, and green indicates the intertill reflection surface. (b) Corresponding AeroTEM resistivity models. (c) Interpreted models.

that lack any defining contrast of electrical properties. Our observations of the valley structures do not preclude that eskers are present in the area. We considered that eskers can coexist with tunnel valleys sometimes following the valley floors (Pugin et al., 2014), sometimes lying upon their shoulders (Jørgensen and Sandersen, 2006), but we do not observe these features from the recovered 1D resistivity models. Eskers are generally much smaller than tunnel valleys, up to approximately 30 m high and 200 m wide. Such features are close to the limit of what can be resolved in our data, especially if they are buried at depths of more than 25–50 m.

As such, our voxel-based segmentation represents an electric property model that represents some, but not all, of the variability in lithology. For example, it is particularly difficult to distinguish any variability within the regional till package, although we know that it is comprised of multiple generations of glacial deposits. Nevertheless, our data are weak in early time gates (near surface), and this may limit our ability to pick actual valley tops.

In addition, given the observed variation of resistivity for the tunnel valleys, it is likely that some tunnel valleys remain indistinguishable from the general till package, and thus they remain undetected.

This concept is similar to that applied in hydrogeology in which several stratigraphically or lithologically distinct units with similar hydrogeologic properties may be represented by a single hydrogeologic unit (e.g., Cummings et al., 2012). We rationalize that for geologic modeling with hydrogeologic intentions, our electric property model is more akin to a hydrogeologic model than a lithological model in that tunnel valleys that are indistinguishable from till or even bedrock do not represent potential aquifers, and so there is little impact on hydrogeologic modeling if they remain undetected. Similarly, a weakly resistive valley signature may result from silty/sandy till fill, or till with small amounts of sand and gravel, but the valley will have less groundwater potential regardless. This will not be the case for all modeling efforts or all contexts.

Our approach is bolstered by the availability of high-quality supporting data, such as seismic reflection and borehole logs. In particular, seismic data provide an important control on bedrock topography. The bedrock surface would be difficult to define based on resistivity alone due to model smoothness and overestimation of

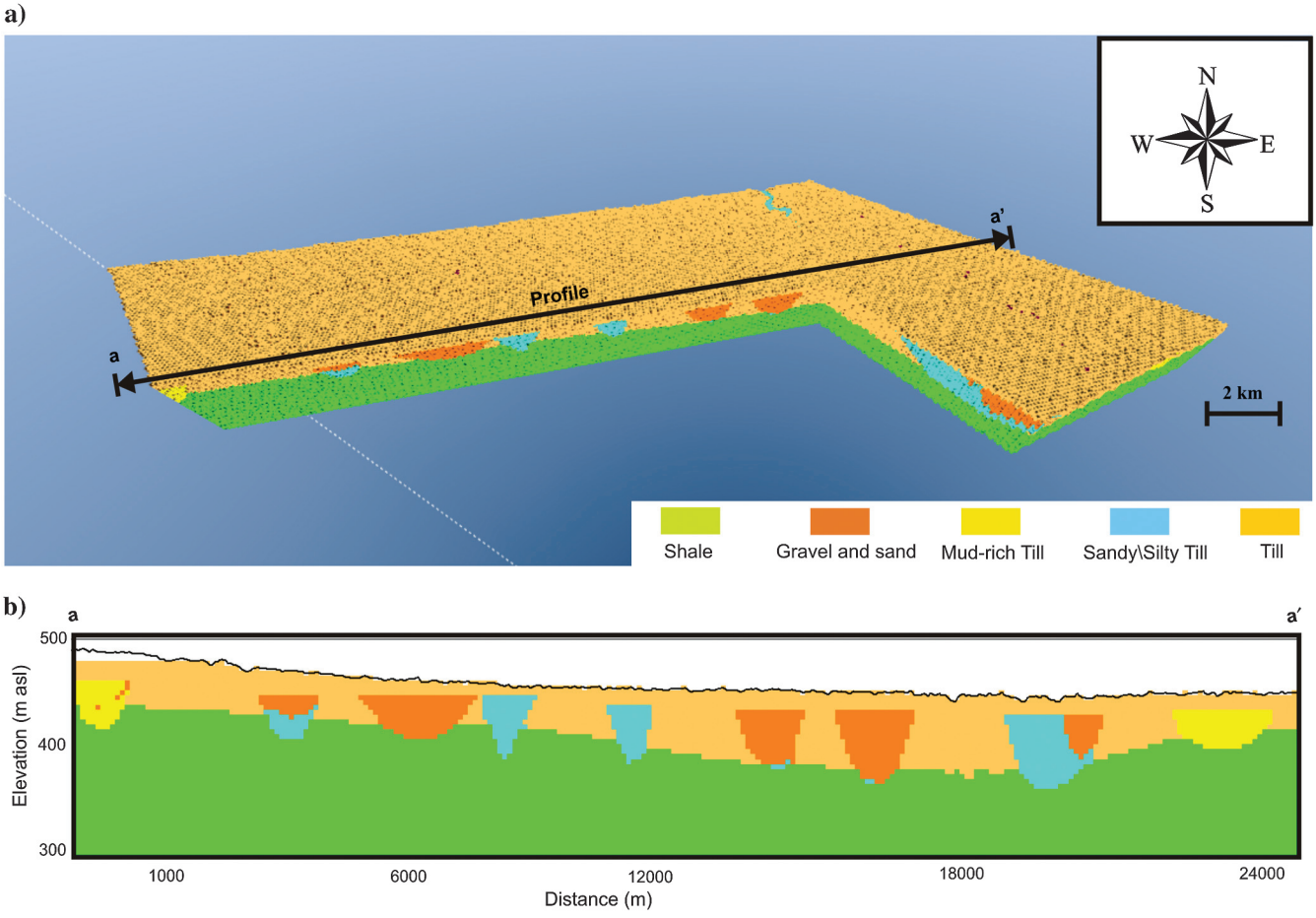

Figure 12. (a) Three-dimensional voxel-based lithological model of a selected portion of the Spiritwood survey area. (b) East–west cross section along M1. The solid black line is the surface topography.

valley depth. Where available, seismic data could be used to better constrain picking of control points, but generally, seismic data are not nearly dense enough for this to be a viable solution for regional 3D modeling of buried valleys geology.

In addition, the seismic data are useful for establishing genetic relationships between the buried valleys because erosional surfaces may be evident as seismic reflections or facies changes that are not accompanied by resistivity contrasts. In some cases, the seismic data provide the uppermost control surface for buried valleys that subtend from the till package. In other cases, the top erosional surface must be interpreted from the resistivity model alone and the location is less certain. In some cases, the seismic data indicate sand or gravel, whereas the AEM resistivity model shows no appreciable resistivity anomaly. In these cases, we lack the ground truth to resolve the discrepancy. The dependence of the resulting model on data type and resolution is well illustrated using the VTEM data set. With the early time data provided by the VTEM survey, we are able to resolve a thin layer interpreted to be mud-rich overlying two buried valleys. This enhanced resolution is important, in that a thin mud-rich layer may decrease surface recharge to buried valley aquifers, or act as a protective cap in the instance of potential surface contamination. However, this particular model unit is an intertill layer and the distinction between mud-rich till and the surrounding till may or may not represent a hydrogeologically significant difference.

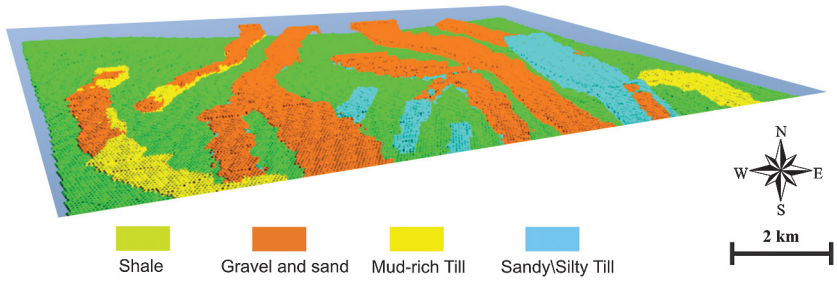

Figure 14. A 3D visualization of the voxel-based geologic model of the buried valleys and the bedrock interpreted at the Spiritwood survey area.

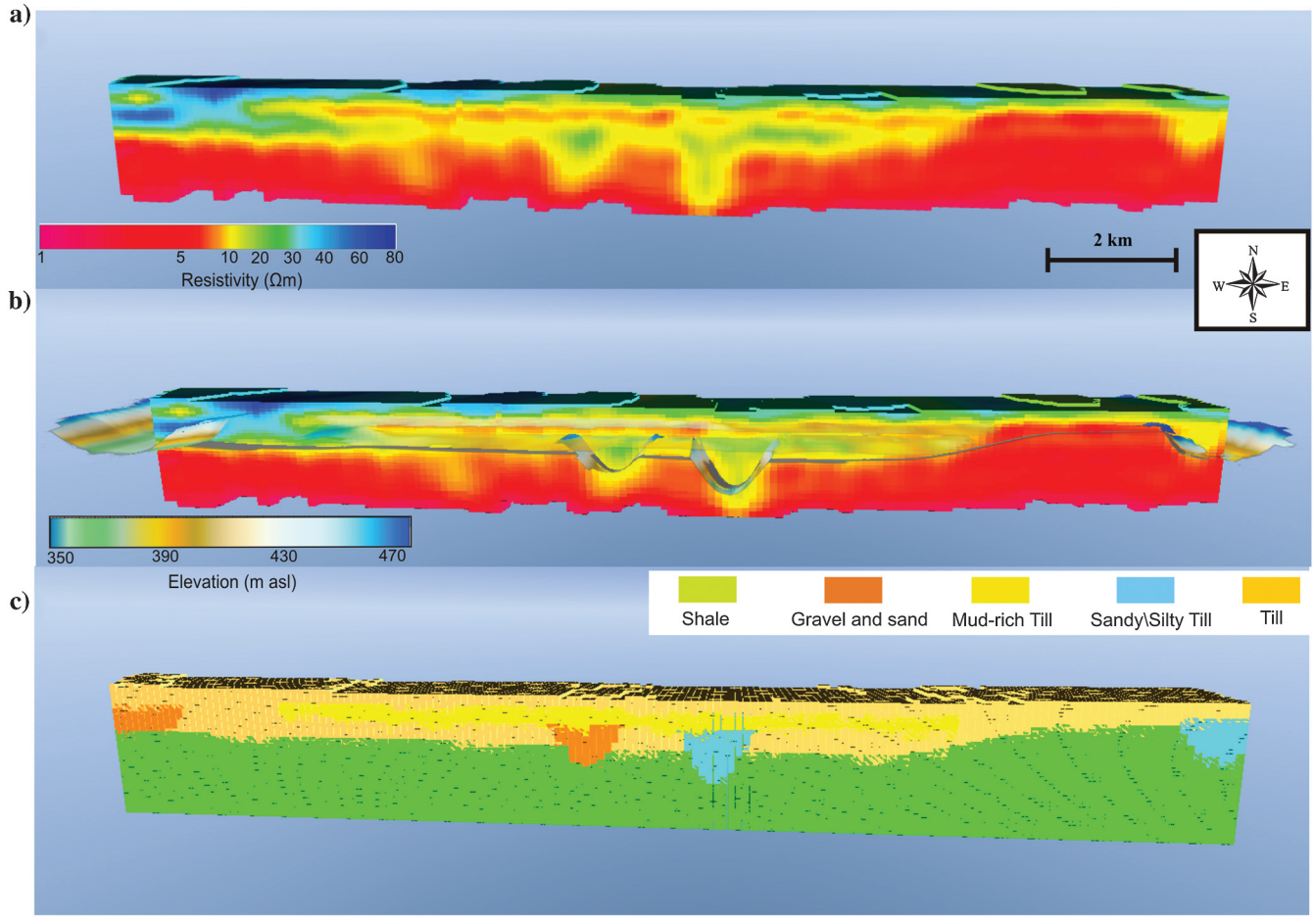

Figure 13. (a) VTEM resistivity model along seismic line S1. (b) A 3D depiction of interpreted surfaces of buried valleys, intertill boundaries and bedrock topography. (c) Voxel-based geologic model.

Conclusion

Regional- and local-scale AEM surveys have been used for 3D interpretation and modeling of a portion of the Spiritwood Buried Valley Aquifer system. Pseudo-3D resistivity models obtained via inversion of the AEM data reveal significant geologic structures that we segment and classify into distinct buried valleys with different morphologies and valley fills. We use a modeling workflow based on a cognitive voxel modeling approach, which incorporates seismic reflection data, borehole geophysical logs, and other supporting knowledge when constructing the model geometry and assigning lithological types. Resistive features are interpreted to be buried valley structures filled with coarse-grained material (sand and gravel) that represent high groundwater resource potential, for which connectivity and volume can be estimated. Our 3D voxel-based model helps to visualize complex 3D geology. In addition, the model takes geophysical data and makes these easily transferable to other disciplines, such as hydrogeology, and more accessible for groundwater management. The cognitive approach allows for construction of a model with sharp contacts and distinct model units from a data set that suffers from smoothness, uncertainty, and a nonunique relationship with lithology.

Acknowledgments

The Spiritwood AeroTEM data set is freely available from Natural Resources Canada. We thank Geotech Ltd. for provision of the VTEM data set. We are grateful to C. Logan, H. Russell, D. Sharpe, M. Hinton, and H. Crow for helpful discussions regarding the Spiritwood Valley. We are thankful to I-GIS for their support and training on the use of the Geoscene 3D software used for the 3D voxel model building. We also thank M. Best, B. Abriel, and an anonymous reviewer for their constructive reviews of our manuscript.

References

Allard, M., 2007, On the origin of the HTEM species: 5th Decennial International Conference on Mineral Exploration, Extended Abstracts, 355–374.

Auken, E., A. V. Christiansen, L. Jacobsen, and K. I. Sørensen, 2008, A resolution study of buried valleys using laterally constrained inversion of TEM data: Journal of Applied Geophysics, **65**, 10–20, doi: 10.1016/j.jappgeo.2008.03.003.

Auken, E., F. Jørgensen, and K. I. Sørensen, 2003, Large-scale TEM investigation for groundwater: Exploration Geophysics, **33**, 188–194, doi: 10.1071/EG03188.

Berg, C. B., S. J. Mathers, H. Kessler, and D. A. Keefer, 2011, Synopsis of current three-dimensional geological mapping and modeling in geological survey organizations: Illinois State Geological Survey, Circular 578.

Betcher, R. N., G. Matille, and G. Keller, 2005, Yes Virginia, there are buried valley aquifers in Manitoba: 58th Canadian Geotechnical Conference, Extended Abstracts, 6E-519.

Christiansen, A. V., N. Foged, and E. Auken, 2014, Inverting for lithology using resistivity models and boreholes: 20th European Meeting of Environmental and Engineering Geophysics, Extended Abstracts, 14–18.

Crow, H. L., R. D. Knight, B. E. Medioli, M. J. Hinton, A. Plourde, A. J. M. Pugin, K. D. Brewer, H. A. J. Russell, and D. R. Sharpe, 2012, Geological, hydrogeological, geophysical, and geochemistry data from a cored borehole in the Spiritwood buried valley, southwest Manitoba: Geological Survey of Canada, Open file 7079.

Cummings, D. I., H. A. J. Russell, and D. R. Sharpe, 2012, Buried-valleys in the Canadian prairies: Geology, hydrogeology, and origin: Canadian Journal of Earth Sciences, **49**, 987–1004, doi: 10.1139/e2012-041.

Danielsen, J. E., E. Auken, F. Jørgensen, V. H. Søndergaard, and K. I. Sørensen, 2003, The application of the transient electromagnetic method in hydrogeophysical surveys: Journal of Applied Geophysics, **53**, 181–198, doi: 10.1016/j.jappgeo.2003.08.004.

Farquharson, C. G., and D. W. Oldenburg, 1993, Inversion of time-domain electromagnetic data for a horizontally layered earth: Geophysical Journal International, **114**, 433–442, doi: 10.1111/j.1365-246X.1993.tb06977.x.

Foged, N., E. Auken, A. V. Christiansen, and K. I. Sørensen, 2013, Test site calibration and validation of airborne and ground based TEM-systems: Geophysics, **78**, no. 2, E95–E106, doi: 10.1190/geo2012-0244.1.

Fountain, D., 2008, 60 years of airborne EM: Focus on the last decade: Presented at 5th International Conference on Airborne Electromagnetics.

Gabriel, G., R. Kirsch, B. Siemon, and H. Wiederhold, 2003, Geophysical investigation of buried Pleistocene sub-glacial valleys in Northern Germany: Journal of Applied Geophysics, **53**, 159–180, doi: 10.1016/j.jappgeo.2003.08.005.

Goldman, M., L. Tabarovsky, and M. Rabinovich, 1994, On the influence of 3-D structures in the interpretation of transient electromagnetic sounding data: Geophysics, **59**, 889–901, doi: 10.1190/1.1443648.

Gunnink, J. L., and S. Bernhard, 2015, Applying airborne electromagnetics in 3D stochastic geohydrological modelling for determining groundwater protection: Near Surface Geophysics, **13**, 45–60, doi: 10.3997/1873-0604.2014044.

Gunnink, J. L., J. H. A. Bosch, B. Siemon, B. Roth, and E. Auken, 2012, Combining ground-based and airborne EM through artificial neural networks for modeling glacial till under saline ground-water conditions: Hydrology and Earth System Sciences, **16**, 3061–3074, doi: 10.5194/hess-16-3061-2012.

Gunnink, J. L., and B. Siemon, 2009, Combining airborne electromagnetic and drillings to construct a stochastic 3D lithological model: 15th European Meeting of Environmental and Engineering Geophysics, EAGE, Extended Abstracts, B02.

Høyer, A. S., F. Jørgensen, N. Foged, X. He, and A. V. Christiansen, 2015, Three-dimensional geological modelling of AEM resistivity data: A comparison of three methods: Journal of Applied Geophysics, **115**, 65–78, doi: 10.1016/j.jappgeo.2015.02.005.

Høyer, A. S., H. Lykke-Andersen, F. Jørgensen, and E. Auken, 2011, Combined interpretation of SkyTEM and high-resolution seismic data: Physics and Chemistry of the Earth, **36**, 1386–1397, doi: 10.1016/j.pce.2011.01.001.

Jørgensen, F., A. S. Høyer, P. B. E. Sandersen, X. He, and N. Foged, 2015, Honouring different data types and geological complexity in a 3D geological model: Computers & Geosciences, **81**, 53–63, doi: 10.1016/j.cageo.2015.04.010.

Jørgensen, F., H. Lykke-Andersen, P. B. E. Sandersen, E. Auken, and E. Nørmark, 2003, Geophysical investigations of buried Quaternary valleys in Denmark: An integrated application of transient electromagnetic soundings, reflection seismic surveys and exploratory drillings: Journal of Applied Geophysics, **53**, 215–228, doi: 10.1016/j.jappgeo.2003.08.017.

Jørgensen, F., R. R. Møller, L. Nebel, N. P. Jensen, A. V. Christiansen, and P. B. E. Sandersen, 2013, A method for cognitive 3D geological voxel modeling of AEM data: Bulletin of Engineering Geology and the Environment, **72**, 421–432, doi: 10.1007/s10064-013-0487-2.

Jørgensen, F., R. R. Møller, P. B. E. Sandersen, and L. Nebel, 2010, 3-D geological modeling of the Egebjerg area, Denmark, based on hydrogeophysical data: Geological Survey of Denmark and Greenland Bulletin, **20**, 27–30.

Jørgensen, F., and P. B. E. Sandersen, 2006, Buried and open tunnel valleys in Denmark: Erosion beneath multiple ice sheets: Quaternary Science Reviews, **25**, 1339–1363, doi: 10.1016/j.quascirev.2005.11.006.

Jørgensen, F., and P. B. E. Sandersen, 2009, Buried Valley mapping in Denmark: Evaluating mapping method constraints and the importance of data density: Zeitschrift der Deutschen Gesellschaft für Geowissenschaften, **160**, 211–223.

Jørgensen, F., P. B. E. Sandersen, and E. Auken, 2003, Imaging buried Quaternary valleys using the transient electromagnetic method: Journal of Applied Geophysics, **53**, 199–213, doi: 10.1016/j.jappgeo.2003.08.016.

Jørgensen, F., P. B. E. Sandersen, E. Auken, H. Lykke-Andersen, and K. Sørensen, 2005, Contributions to the geological mapping of Mors, Denmark: A study based on a large-scale TEM survey: Bulletin of the Geological Society of Denmark, **52**, 53–75.

Kaufmann, O., and T. Martin, 2008, 3D geological modeling from boreholes, cross-sections and geological maps, application over former natural gas storages in coal mines: Computers & Geosciences, **34**, 278–290, doi: 10.1016/j.cageo.2007.09.005.

Kehew, A. E., and W. M. Boettger, 1986, Depositional environments of buried-valley aquifers in North Dakota: Ground Water, **24**, 728–734, doi: 10.1111/j.1745-6584.1986.tb01688.x.

Kluiving, S. J., J. H. A. Bosch, J. H. J. Ebbing, C. S. Mesdag, and R. S. Westerhoff, 2003, Onshore and offshore seismic and lithostratigraphic analysis of a deeply incised Quaternary buried valley-system in the Northern Netherlands: Journal of Applied Geophysics, **53**, 249–271, doi: 10.1016/j.jappgeo.2003.08.002.

Legault, J. M., A. Prikhodko, D. J. Dodds, J. C. Macnae, and G. A. Oldenborger, 2012, Results of recent VTEM helicopter system development testing over the Spiritwood Valley aquifer, Manitoba: 25th Symposium on the Application of Geophysics to Engineering and Environmental Problems, EEGS, Expanded Abstracts, 17.

Logan, C. E., M. J. Hinton, D. R. Sharpe, G. A. Oldenborger, H. A. J. Russell, and A. J-M. Pugin, 2015, Spiritwood Buried Valley 3D geological modelling: Part of a multidisciplinary aquifer characterization workflow: Geological Survey of Canada, Open file 7866.

Marker, P. A., N. Foged, A. V. Christiansen, E. Auken, and P. Bauer-Gottwein, 2014, Automatic generation of groundwater model hydrostratigraphy from AEM resistivity and boreholes: 20th European Meeting of Environmental and Engineering Geophysics, Extended Abstracts, 9–13.

Oldenborger, G. A., and K. Brewer, 2014, Time-domain electromagnetic data for the Spiritwood Valley Aquifer, Manitoba: Geological Survey of Canada, Open file 7593.

Oldenborger, G. A., C. E. Logan, M. J. Hinton, V. Sapia, A. J.-M. Pugin, D. R. Sharpe, A. I. Calderhead, and H. A. J. Russell, 2014, 3D hydrogeological model building using airborne electromagnetic data: 20th European Meeting of Environmental and Engineering Geophysics, Tu-PA1-07.

Oldenborger, G. A., A. J. M. Pugin, and S. E. Pullan, 2013, Airborne time-domain electromagnetics, electrical resistivity and seismic reflection for regional three-dimensional mapping and characterization of the Spiritwood Valley Aquifer, Manitoba, Canada: Near Surface Geophysics, **11**, 63–74, doi: 10.3997/1873-0604.2012023.

Paine, J. G., and B. R. S. Minty, 2005, Airborne hydrogeophysics, *in* Y. Rubin, and S. S. Hubbard, eds., Hydrogeophysics: Springer, Water Science and Technology Library 50, 333–357.

Palacky, G. J., 1988, Resistivity characteristics of geologic targets, *in* M. N. Nabighian, ed., Electromagnetic methods in applied geophysics: SEG Investigations in Geophysics, 53–129.

Podgorski, J. E., E. Auken, C. Schamper, A. V. Christiansen, T. Kalscheuer, and A. G. Green, 2013, Processing and inversion of commercial helicopter time-domain electromagnetic data for environmental assessments and geologic and hydrologic mapping: Geophysics, **78**, no. 4, E149–E159, doi: 10.1190/geo2012-0452.1.

Pryet, A., J. Ramm, J. P. Chiles, E. Auken, B. Deffontaines, and S. Violette, 2011, 3D resistivity gridding of large AEM datasets: A step-toward enhanced geological interpretation: Journal of Applied Geophysics, **75**, 277–283, doi: 10.1016/j.jappgeo.2011.07.006.

Pugin, A. J. M., G. A. Oldenborger, D. I. Cummings, H. A. Russell, and D. R. Sharpe, 2014, Architecture of buried valleys in glaciated Canadian Prairie regions based on high resolution geophysical data: Quaternary Science Reviews, **86**, 13–23, doi: 10.1016/j.quascirev.2013.12.007.

Pugin, A. J.-M., G. A. Oldenborger, and S. Pullan, 2011, Buried Valley imaging using 3-C seismic reflection, electrical resistivity and AEM surveys: 24th Symposium on the Application of Geophysics to Engineering and Environmental Problems, Extended Abstracts, 1–7.

Raiber, M., P. A. White, C. J. Daughney, C. Tschritter, P. Davidson, and S. E. Bainbridge, 2012, Three-dimensional geological modeling and multivariate statistical analysis of water chemistry data to analyse and visualise aquifer structure and groundwater composition in the Wairau Plain, Marlborough District, New Zealand: Journal of Hydrology, **436**, 13–34, doi: 10.1016/j.jhydrol.2012.01.045.

Randich, P. G., and R. L. Kuzniar, 1984, Geology of Towner County, North Dakota: North Dakota State Water Commission, County Groundwater Studies 36, Part III.

Royse, K. R., 2010, Combining numerical and cognitive 3D modeling approaches in order to determine the structure of the Chalk in the London Basin: Computers & Geoscience, **36**, 500–511, doi: 10.1016/j.cageo.2009.10.001.

Sapia, V., G. A. Oldenborger, A. Viezzoli, and M. Marchetti, 2014a, Incorporating ancillary data into the inversion of airborne time-domain electromagnetic data for hydrogeological applications: Journal of Applied Geophysics, **104**, 35–43, doi: 10.1016/j.jappgeo.2014.02.009.

Sapia, V., A. Viezzoli, F. Jørgensen, G. A. Oldenborger, and M. Marchetti, 2014b, The impact on geological and hydrogeological mapping results of moving from ground to airborne TEM: Journal of Environmental and Engineering Geophysics, **19**, 53–66, doi: 10.2113/JEEG19.1.53.

Sattel, D., 2009, An overview of helicopter time-domain EM systems: 20th Geophysical Conference, ASEG, Extended Abstracts, 1–6.

Schamper, C., F. Jørgensen, E. Auken, and F. Effersø, 2014, Assessment of near-surface mapping capabilities by airborne transient electromagnetic data: An extensive comparison to conventional borehole data: Geophysics, **79**, no. 4, B187–B199, doi: 10.1190/geo2013-0256.1.

Scharling, P. B., E. S. Rasmussen, T. O. Sonnenborg, P. Engesgaard, and K. Hinsby, 2009, Three-dimensional regional-scale hydrostratigraphic modeling based on sequence stratigraphic methods: A case study of the Miocene succession in Denmark: Hydrogeology Journal, **17**, 1913–1933, doi: 10.1007/s10040-009-0475-6.

Shaver, R. B., and S. W. Pusc, 1992, Hydraulic barriers in Pleistocene buried-valley aquifers: Ground Water, **30**, 21–28, doi: 10.1111/j.1745-6584.1992.tb00807.x.

Sheets, R. A., and K. E. Bossenbroek, 2005, Ground-water flow directions and estimation of aquifer hydraulic properties in the lower Great Miami river buried valley aquifer system, Hamilton area, Ohio: USGS Scientific Investigations Report 2005–2013.

Thomson, S., D. Fountain, and T. Watts, 2007, Airborne geophysics: Evolution and revolution: Fifth Decennial International Conference on Mineral Exploration, Exploration 07, Extended Abstracts, 19–37.

Venteris, E. R., 2007, Three-dimensional modeling of glacial sediments using public water-well data records: An integration of interpretive and geostatistical approaches: Geosphere, **3**, 456–468, doi: 10.1130/GES00090.1.

Viezzoli, A., A. V. Christiansen, E. Auken, and K. Sørensen, 2008, Quasi-3D modeling of airborne TEM data by spatially constrained inversion: Geophysics, **73**, no. 3, F105–F113, doi: 10.1190/1.2895521.

Viezzoli, A., F. Jørgensen, and K. Sørensen, 2013, Flawed processing of airborne EM data affecting hydrogeological interpretation: Ground Water, **51**, 191–202, doi: 10.1111/j.1745-6584.2012.00958.x.

Wiecek, S., 2009, Municipality of Killarney, Turtle Mountain groundwater assessment study: W.L. Gibbons & Associates, Inc.

Winter, T. C., R. D. Benson, R. A. Engberg, G. J. Wiche, D. G. Emerson, O. A. Crosby, and J. E. Miller, 1984, Synopsis of ground-water and surface-water resources of North Dakota: United States Geological Survey, Open File Report 84–732.

Vincenzo Sapia graduated in geology from the University of Rome III. He received a Ph.D. (2014) in advanced modeling of time-domain electromagnetic data from Alma Mater Studiorum University of Bologna. To date, he is in a postdoc position at the Istituto Nazionale di Geofisica e Vulcanologia. Since 2008, his main research interests include electrical, magnetic, and frequency-domain methods for disposal sites and archaeological investigations in addition to time-domain electromagnetic geophysics and electrical tomography applied to geologic, hydrogeological, and geotechnical investigations. He is interested in many aspects of airborne electromagnetic methods, from data processing and inversion to data interpretation and 3D modeling. He is the author or coauthor of more than 30 scientific papers and extended abstracts from conferences worldwide.